Cellular interface morphologies in directional solidification.
II. The effect of grain boundaries

Lyle H. Ungar and Robert A. Brown*

*Department of Chemical Engineering and Materials Processing Center, Massachusetts Institute of Technology,
Cambridge, Massachusetts 02139*

Grain boundaries along a planar melt/solid interface significantly affect the onset and small-amplitude development of morphological instabilities during the solidification of a binary alloy. A singular perturbation analysis valid for small grain-boundary slopes is used with the one-sided model for solidification to show that grain boundaries introduce imperfections into the symmetry of the developing cellular interfaces which rupture the junction between the family of planar shapes and the bifurcating cellular families. Undulating interfaces are shown to develop first near grain boundaries, in agreement with experiments, and to evolve with decreasing temperature gradient either by a smooth transition from the almost planar family or by a sudden jump to moderate-amplitude cellular forms, depending on the growth rate. Finite-element calculations for the Pb-Sb system give interface shapes for the large grain-boundary slopes which are typically observed.

I. INTRODUCTION

The microscopic transitions in spatial pattern of a solidifying melt/solid have been the subject of intense theoretical and experimental research because of the fundamental importance of these structures in the physical and electrical properties of materials and because these interface morphologies represent an excellent example of pattern formation in nature. The linear theory of Mullins and Sekerka[1,2] and subsequent nonlinear analyses[3-8] have established the initial stages of the evolution between a planar solidification front and large-amplitude cellular interfaces. In a recent paper (Ref. 8; henceforth referred to as I) we have used ideas from bifurcation theory to describe this transition in terms of changes in the temperature gradient. When the temperature gradient is exactly constant away from the interface, a planar shape is a steady-state form for all values of $\tilde{G}$. Cellular interfaces evolve from bifurcations located at the neutral stability points $\tilde{G} = \tilde{G}_c$ determined by Mullins and Sekerka; see Ref. 8. Families of cellular interfaces develop from the planar forms and evolve toward either increasing (subcritical bifurcation) or decreasing (supercritical bifurcation) temperature gradient, depending on the growth rate and thermophysical properties of the melt and solid. These two cases are shown schematically in Fig. 2 as a plot of the amplitude of the interface deflection measured by ϵ as a function of the temperature gradient $\tilde{G}$.

Much experimental research has been directed at confirming the predictions of these theories for the onset of morphological instability. Several of these studies have noted the pronounced tendency for the instability to form first near the three-phase junctions where grain boundaries intersect the solidification front,[9-12] shown schematically in Fig. 1. Large-amplitude undulations in interface shape have been observed about these intersections at temperature gradients or growth rates just before

the critical values predicted by the linear theory in Refs. 1 and 2. The purpose of this paper is to explain this observation theoretically and to put into perspective the role of imperfections in interface shape caused by grain boundaries.

We consider the solidification of a binary melt in an imposed constant temperature gradient which is not disturbed by deformation of the melt/solid interface. This is precisely the case for a material with almost equal thermal conductivities in melt and solid and negligible latent heat of solidification. These assumptions lead to the "one-sided" model for solidification described in I. The conclusions described in this paper are qualitatively correct for the more complicated model treated by Mullins and Sekerka which lifts these two restrictions by solving simultaneously for the temperature field; this point is discussed further in Sec. V.

Coriell and Sekerka[13,14] extended the linear analysis of Mullins and Sekerka to steadily solidifying interfaces with a single grain boundary by constructing a regular perturbation for small grain angles. They concluded that the interface would deform more close to the grain boundary, but failed to predict any change in the critical value of $\tilde{G}$ for the onset of the instability. We show that the regular
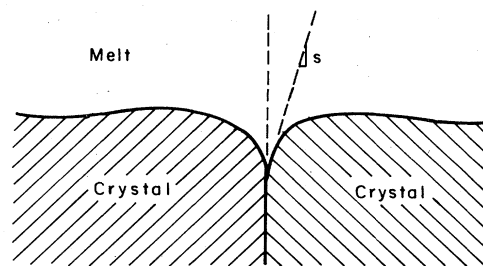

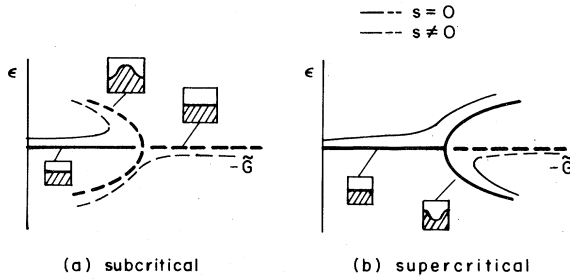FIG. 1. Schematic of melt/solid interface with a grain boundary with slope s.

FIG. 2. Families of small-amplitude cellular interfaces characterized as either subcritical or supercritical bifurcation in terms of $-G$. Curves for nonzero s represent imperfections caused by grain angle.

perturbation in slope used in Refs. 13 and 14 fails close to the marginal stability point and that a singular analysis is necessary to explain the interaction between this limit and the interface deformation caused by a grain boundary.

The singular perturbation analysis used here is based on well-established methods in bifurcation theory[15−17] for describing imperfections in solution structure near a bifurcation point caused by introducing a second parameter which disrupts the symmetry of the bifurcating family. Introducing a grain angle along the melt/solid interface destroys the reflective symmetry between the two phases that exists for a planar interface and acts as an imperfection to the bifurcations. The singular change in solution structure about this point caused by small values of s is portrayed in Fig. 2.

The effect of the grain boundary is different for subcritical and supercritical bifurcations. When the cellular interfaces evolve supercritically, i.e., to lower values of $\tilde{G}$, the grain boundary ruptures the intersection of the planar and cellular families into a curve of stable shapes, single valued in $\tilde{G}$, and a separate arc of solutions. Undulations will develop slowly in the interface and no value of $\tilde{G}$ can be identified as $\tilde{G}_c$. When the bifurcation is subcritical the grain boundary causes the family of originally planar shapes to terminate abruptly at a limit point, where it turns back to higher values of $\tilde{G}$. As is shown in Sec. III, this point shifts according to $s^{2/3}$.

The one-sided model used here was developed in I, and only its mathematical statement is repeated in Sec. II along with relevant results of the linear analysis. The nonlinear perturbation analysis is contained in Sec. III. Finally, the results of finite-element calculations, using the methods presented in I, are presented in Sec. IV to show the effect of the grain angle on moderate-amplitude cellular interface shapes.

II. ONE-SIDED MODEL AND LINEAR STABILITY ANALYSIS

The one-sided solidification model presented in I for the solute concentration $\tilde{c}(\tilde{x},\tilde{y},\tilde{t})$ and the melt/solid interface shape $\tilde{h}(\tilde{x},\tilde{t})$ is written in terms of the conservation equation

$$\frac{\partial \tilde{c}}{\partial t} = \mathscr{D}\tilde{\nabla}^2\tilde{c} + V\frac{\partial \tilde{c}}{\partial y} , \tag{2.1}$$

where $\mathscr{D}$ is the diffusion coefficient. This solute balance is solved inside the melt region $(0 \leq \tilde{x} \leq \tilde{\lambda},$ $\tilde{h}(\tilde{x},\tilde{t}) \leq \tilde{y} \leq \infty)$. Along the sides of the slice and far away, the solute field has the boundary conditions

$$\tilde{c}_x(0,\tilde{y}) = \tilde{c}_x(\tilde{\lambda},\tilde{y}) = 0 , \quad \tilde{y} = (0,\infty) \tag{2.2}$$

$$\tilde{c}(\tilde{x},\infty) = c_\infty , \tag{2.3}$$

where c_∞ is the bulk concentration of solute. The two conditions written along the melt/solid interface are the solute balance

$$\vec{\mathbf{n}} \cdot \vec{\tilde{\nabla}} c = \vec{\mathbf{n}} \cdot \vec{\mathbf{e}}_y V \tilde{c}(k-1) , \tag{2.4}$$

where $\vec{\mathbf{e}}_y$ is the unit vector in the y direction and the temperature condition constructed from an idealized phase diagram

$$T_I = T_m + \tilde{m}c + 2\tilde{\Gamma}\mathscr{H} . \tag{2.5}$$

In these conditions, k is the segregation coefficient, $\tilde{m}$ is the slope of the liquidus curve, $\tilde{\Gamma}$ is the capillary length, T_m is the melting temperature of the pure material at a planar interface, and $2\mathscr{H} = \tilde{h}_{xx}(1+\tilde{h}_x^2)^{-3/2}$ is the mean curvature of the interface. We solve these equations with the boundary conditions on the interface that prescribe a symmetry plane at $\tilde{x} = \tilde{\lambda}$ and the grain angle s at $\tilde{x} = 0$:

$$\frac{\partial \tilde{h}}{\partial x} = s , \quad \tilde{x} = 0 , \quad \frac{\partial \tilde{h}}{\partial x} = 0 , \quad \tilde{x} = \tilde{\lambda} , \quad 0 \leq \tilde{y} \leq \infty . \tag{2.6}$$

These conditions describe a periodic array of grains along the interface separated by a distance $2\tilde{\lambda}$. In the limit $s \to 0$, the free boundary problem composed of Eqs. (2.1)−(2.6) reduces to the equation set used in I to describe the development of cellular interfaces from a planar solidification front.

For small values of s, the linear stability analysis of the planar interface follows by expanding the equations about the flat interface and collecting terms $O(s)$. Following the notation in Ref. 13, the response of the interface to a perturbation of the form $\tilde{h}(\tilde{x},\tilde{t}) = \tilde{h}(\tilde{t})\cos(\tilde{\omega}\tilde{x})$, where $\tilde{\omega} = 2\pi/\tilde{\lambda}$ is the spatial wave number, is given by

$$\tilde{h}(\tilde{x},\tilde{t}) = \cos(\tilde{\omega}\tilde{x})\{\exp(f(\tilde{\omega})\tilde{t})$$

$$+ s[g(\tilde{\omega})/f(\tilde{\omega})][\exp(f(\tilde{\omega})\tilde{t})-1]\} , \tag{2.7}$$

where $f(\tilde{\omega})$ and $g(\tilde{\omega})$ are defined as

$$f(\tilde{\omega}) \equiv \frac{-(\tilde{G}+T_m\tilde{\Gamma}\tilde{\omega}^2)\mathscr{D}K(\tilde{\omega}^*-V(1-k)/\mathscr{D})}{\tilde{m}c_\infty(k-1)}$$

$$+ V(\tilde{\omega}^*-V/\mathscr{D}) , \tag{2.8}$$

$$g(\tilde{\omega}) \equiv \frac{T_m\tilde{\Gamma}\mathscr{D}k(\tilde{\omega}^*-V(1-k)/\mathscr{D})}{\tilde{m}c_\infty(k-1)} , \tag{2.9}$$

with $\tilde{\omega}^* \equiv V/2\mathscr{D} + [(V/2\mathscr{D})^2+\tilde{\omega}^2]^{1/2}$. The first term in Eq. (2.7) is identical to Mullins and Sekerka's result for a perfectly periodic interface, whereas the second term arises as a correction due to the presence of the grain

boundary. The function $f(\tilde{\omega})$ dictates the stability of the interface. The wave number $\tilde{\omega}=\tilde{\omega}_c$ for which instability starts at the largest value of $\tilde{G}$ corresponds to the most dangerous instability to the planar form. We focus on this disturbance in most of our analysis.

Because $f(\tilde{\omega})$ is independent of s, it appears that the marginal stability curve is independent of the small grain angle. However, $f(\tilde{\omega})$ appears in the denominator of the second term of Eq. (2.7). This term is infinite for any nonzero value of s as the neutral stability point is approached and implies that the regular perturbation expansion in s used here and in Refs. 13 and 14 is not valid close to the onset of the instability. The correct scaling for the first-order correction in the grain-boundary slope is the subject of the next section.

III. ASYMPTOTIC ANALYSIS OF IMPERFECT BIFURCATION

The behavior of the solution structure close to the bifurcation point is captured by rescaling the equation set to remove the singularity in the parameter s. To do this in terms of the amplitude expansion developed in I for the problem with $s=0$, we redefine the interface shape function $\tilde{h}(\tilde{x},\tilde{t})$ to remove the dependence on s from the boundary condition (2.7) by the substitution

$$\tilde{h}(\tilde{x})\equiv\tilde{H}(\tilde{x})+s\tilde{F}(\tilde{x}) , \tag{3.1}$$

where $\tilde{F}(\tilde{x})$ satisfies the conditions

$$\left.\frac{\partial\tilde{F}}{\partial\tilde{x}}\right|_{\tilde{x}=0}=1 , \quad \left.\frac{\partial\tilde{F}}{\partial\tilde{x}}\right|_{\tilde{x}=\tilde{\lambda}}=0 , \tag{3.2}$$

but is otherwise arbitrary.

The equation set (2.1)–(2.9) with the modified boundary condition Eq. (3.1) is made dimensionless by scaling length with λ^*, concentration with c_∞, and temperature with T_m^0. The dimensionless versions of these variables are denoted by dropping the tilde from each symbol. The steady-state version of these equations is

$$\nabla^2 c + P\frac{\partial c}{\partial z}=0 , \tag{3.3a}$$

$$G(H+sF)-m\frac{(k-1)}{k}(1-e^{-P(H+sF)})-mc$$
$$-\Gamma(H_{xx}+F_{xx})(1+H_x^2+F_x^2)^{-3/2}=0 , \tag{3.3b}$$

$$c_y-H_xF_xc_x-(k-1)P(c+1-e^{-P(H+sF)})=0 , \tag{3.3c}$$

with the boundary conditions

$$H_x(0)=0 , \quad H_x(\lambda)=c_x(0,y)=c_x(\lambda,y)=0 . \tag{3.3d}$$

In these equations, $P=V\lambda^*/\mathscr{D}$ is the Peclet number, $\Gamma=\tilde{\Gamma}/\lambda^*$ is the capillary constant, $G=\tilde{G}\lambda^*/T_m^0$ is the dimensionless temperature gradient, $m=\tilde{m}c_\infty/T_m^0$ is the slope of the phase diagram, and λ is the dimensionless wavelength. In Eqs. (3.3) the subscripts x and y denote partial differentiation.

The proper dependence of the field variables and temperature gradient on the grain slope as s approaches zero is computed by expanding the variables (c,H) and the parameters (G,s) about the neutral stability point in a power series written in terms of a scaling parameter δ:

$$\begin{bmatrix} c(x,y,\delta) \\ H(x,\delta) \\ G(\delta) \\ s(\delta) \end{bmatrix} = \sum_{n=0}^{\infty}\frac{\delta^n}{n!}\begin{bmatrix} c^{(n)}(x,y) \\ H^{(n)}(x) \\ G_n \\ s_n \end{bmatrix} . \tag{3.4}$$

The form of the equation sets recovered at each order of δ is practically identical to those in the perturbation analysis for the planar interface $(s=0)$ given in I. The linear problem at each order of δ has the form

$$\underline{u}_n=\underline{\rho}_n+\underline{\rho}_{ns} , \tag{3.5}$$

where $\underline{u}_n\equiv(H(x),c(x,H))^T$ and the operator and the right-hand-side vector $\underline{\rho}_n$ are given by Eqs. (3.5)–(3.6) in I. The only contribution of the grain angle to this sequence occurs in $\underline{\rho}_{ns}$ as

$$\underline{\rho}_{ns}=s_n(F(x),0)^T+O(s_{n-1}) , \tag{3.6}$$

where $O(s_{n-1})$ denotes unspecified terms proportional to s_{n-1}.

Because the linear operator and boundary conditions for each problem do not contain s, the inner product used for the undisturbed interface [see Eq. (3.10) in I] is applied to determine the solvability of each nonhomogeneous problem. The operator $\mathscr{L}$ is singular for $G=G_c$, so that the nonhomogeneous problems are solvable only if

$$\langle\underline{\rho}_n+\underline{\rho}_{ns},\underline{\Phi}^*\rangle=0 , \tag{3.7}$$

where $\{\underline{\Phi}_n^*\}$ are the adjoint eigenfunctions for the undisturbed problem given in Eq. (3.11) of I. At first order in δ, Eq. (3.7) requires that $s_1=0$, verifying that a regular expansion of G_c in s is not appropriate. With $s_1=0$, the first-order solution becomes $\underline{U}_1=A\underline{\Phi}_n$ where the $\{\underline{\Phi}_n\}$ are eigenfunctions of the eigenvalue problem describing stability of the planar interface and are given in Eq. (3.8) of I. These eigenfunctions mark the branch points for families of cellular interfaces with spatial wave number $\omega_n=2n\pi/\lambda$. The constant A in the solution $\underline{U}_1$ is determined along with the solutions to the higher-order problems.

The spacing of the grain boundaries relative to the wavelength of the cellular instability for a planar interface depends on the value of n for the highest value of $G_c^{(n)}$. When n is large, the grain boundaries are widely spaced with respect to this wavelength and, in some sense, our analysis approaches that of Ref. 14 for a single grain boundary.

The solvability condition requires that at $O(\delta^2)$, both G_1 and s_2 be zero. The solution of Eqs. (3.3) is $\underline{U}_2=A^2\underline{u}_2^{(n)}$, where $\underline{u}_2^{(n)}$ is given in Eq. (3.14b) of I. The solvability condition for the third-order problem dictates that s_3 be nonzero. Without loss of generality, we pick this constant to be unity and set all higher values in the expansion $\{s_n\}$, $n>3$, to zero. Then the proper scaling between δ and s is

$$s=\delta^3/3! . \tag{3.8}$$

The form of the solvability constraint at $O(\delta^3)$ is

$$c_1A^3+c_2G_2A+c_3=0 , \tag{3.9}$$

where the constants c_1 and c_2 are the same as those that appeared in the third-order solvability condition for the undisturbed system and $c_3 = \langle \rho_{3s}, \Phi_n^* \rangle = -\omega^{-2}$.

Each of the possible three roots to the amplitude equation (3.9) correspond to a family of interfaces displayed in Fig. 2(b). The limit point where the solution is lost due to an imperfection of a subcritical bifurcation occurs when two roots of Eq. (3.9) coincide for a particular value of G_2. The substitution of this value of G_2 into the expansion for G and the use of Eq. (3.8) gives the value of G for the limit point as

$$G = G_c + 3(\Gamma^2 G_{2I}/2\lambda^2)^{1/3} s^{2/3} , \qquad (3.10)$$

where $G_{2I}^{O(n)}$ is listed in I as Eq. (3.15). For small values the grain angle, Eq. (3.10) predicts a very rapid increase in the value of G for marginal stability with changes in s; this is precisely what has been observed experimentally.

Our singular analysis has been constructed only to model the behavior of each family of interface shapes in the small region $|G - G_c^{(n)}| \ll 1$. Uniformly valid representations for each interface family over the entire range of G, but for small grain angles, can be constructed by the matching procedure outlined in Ref. 16. Here the expansions valid near the critical points for the unperturbed problem are matched to expansions in s for each family valid away from $G_c^{(n)}$. As implied in Fig. 2, the expansions away from the bifurcation points are regular in s. The results of Coriell and Sekerka[14] are the $O(s)$ approximations of this type written about the family of originally ($s = 0$) planar forms. The linear stability of the interface shapes in their calculations are indicative of those shown in Fig. 2.

The analysis in this section is valid for grain boundaries spaced at any integer multiple of the wavelength of the cellular shapes for $s = 0$. To approach Coriell and Sekerka's analysis of a single grain boundary along an otherwise planar interface, we consider the case when $\lambda \gg 1$ for s small, but fixed. For the analysis to remain valid, each term in the third-order solvability condition Eq. (3.9) must be the same size. This constraint applied to the term with the grain angle forces $s \ll \lambda^{-1}$. A similar criterion was developed by Hall and Walton[18] in an analysis of imperfect bifurcation of natural convection in a long, thin cavity heated from below. This limit is severe because it forces the region of validity in s to be infinitesimal as the distance between grain boundaries becomes large.

IV. FINITE-ELEMENT CALCULATIONS

The asymptotic results of the last section are extended to large-amplitude interface deflections and large grain angles by finite-element analysis of Eqs. (3.3). The finite-element–Newton algorithm used for the calculations, as well as the computer-implemented perturbation methods used to trace families of solutions to the discretized set, are described in I and in the references contained therein. We again focus on the thermophysical properties for the Pb-Sb system which are listed in Table I of Ref. 8; these parameters are similar to those used by Coriell and Sekerka[14] except for the assumption of equal conductivi-

ties in melt and solid and zero latent heat release. The reference length is taken as $\lambda^* = 0.01$ cm and the Peclet number is $P = 0.8$, indicative of crystal growth at approximately 16 μm/sec. The capillary constant is $\Gamma = 8.2 \times 10^{-7}$. Calculations are presented for both small and large values of the grain angle s to clarify the connections between the perfect and the imperfect solution structures.

The change in the family of originally planar shapes with increasing grain angle is shown in Fig. 3 for grains spaced periodically at intervals of $\lambda = 2$, which is simultaneously close to the most-dangerous wavelength for instability of a planar form and to the transition between subcritical and supercritical bifurcation (see I). Each interface shape is represented by the maximum deflection Δ

$$\Delta \equiv \max_{0 \leq x \leq \lambda} \{h(x)\} - \min_{0 \leq x \leq \lambda} \{h(x)\} , \qquad (4.1)$$

computed as a function of the dimensionless temperature gradient G. The bifurcation between the planar and cellular shapes for $s = 0$ is shown for reference.

For the small grain angle $s = 0.1$ ($\sim 6°$) the family of shapes evolving from high values of G was easily recognized as the result of rupturing the bifurcation point for the planar family. The interface deflection developed smoothly until, for a temperature gradient less than the value predicted by the linear analysis, the solutions reversed direction in G and lost stability. The family regained stability at a second limit point at higher interface deflection, just as did the family of cellular forms bifurcating from the planar shape; compare to Fig. 4 in I. In this sense, the presence of the grain boundary had little influence on the nonlinear structure of the cellular families.

The solution curves shifted significantly towards higher values of G when the angle was increased to either $s = 1.0$ (45°) or $s = 5.0$ ($\sim 89°$). The limit point had shifted to $G = 1.86 \times 10^{-4}$ for $s = 1.0$ from the value $G = G_1 = 1.75 \times 10^{-4}$ for $s = 0.1$.

A portion of the interface family was still unstable for $s = 1.0$; however, all the shapes were stable for $s = 5.0$
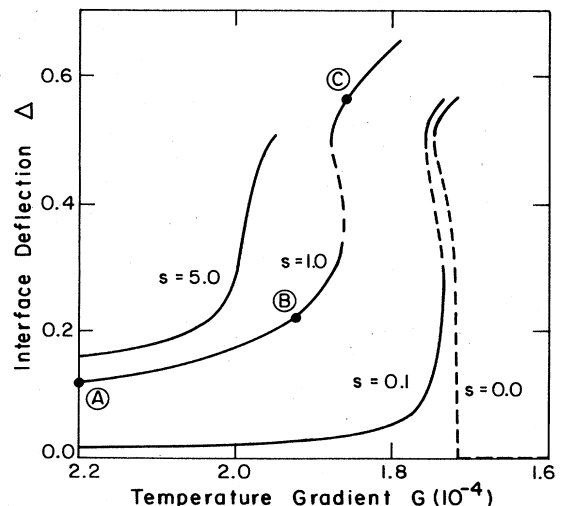
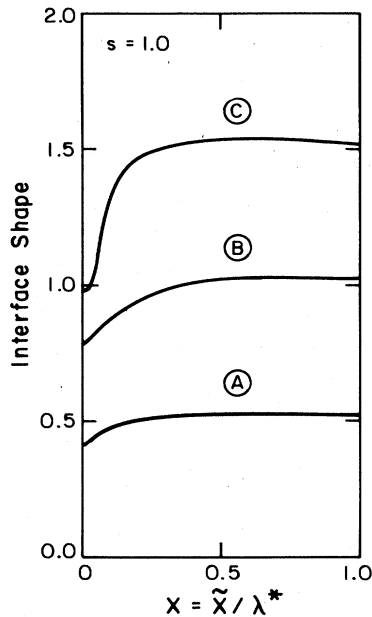FIG. 3. Families of cellular interfaces for $P = 0.8$ and $\lambda = 2.0$ as a function of the grain angle s.

FIG. 4. Sample interface shapes for $s=1.0$. Letters refer to points in Fig. 3.

where the interface deflection increased monotonically with decreasing temperature gradient. Interface shapes corresponding to the points designated along the curve for $s=1.0$ are given as Fig. 4; only one-half wavelength of the interface is shown for each case. The interface developed only a single undulation in the interval $0 \leq x \leq \lambda$ because the primary mode of instability had the same wavelength as the grain-boundary spacing. The deep grooves separating almost planar plateaus were similar to the large-amplitude shapes computed in I without the grains.

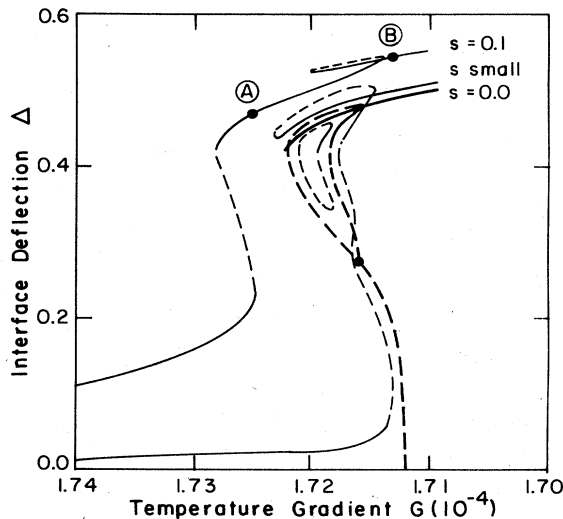The interface shapes seen experimentally show large-amplitude undulations near the grain boundary that de-

FIG. 5. Families of cellular interfaces for $P=0.8$ and $\lambda=4$ for the grain angle $s=0.1$. The curves for $s \ll 1$ are displayed to imply the rupturing of the bifurcating families.
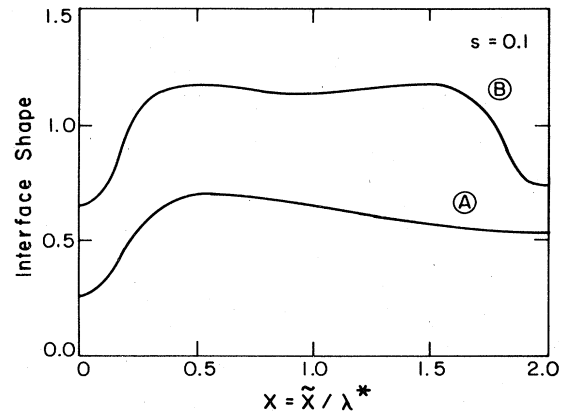

FIG. 6. Sample interface shapes for $s=0.1$ and $2\lambda=4$. Letters correspond to points in Fig. 5.

crease in intensity with distance away from the imperfection. The spacing between the grains was increased to allow for multiple cells to form along each grain in an attempt to see this effect. Increasing the spacing between grain boundaries led to much more complicated solution structures. This was expected from the results in I for bifurcation from the planar interface with $\lambda=4$, where families with shapes of longer wavelength evolved by secondary bifurcation from the families of interfaces with the fundamental wavelengths. The loss in symmetry caused by the presence of the grain angle ruptures these secondary bifurcations as well.

The perfect $(s=0)$ and imperfect $(s\neq0)$ interface families computed for grains spaced $2\lambda=4$ apart are shown in Fig. 5, as calculated with a crude finite-element mesh. The families for a very small value of s are given to show the rupturing of each of the bifurcation points caused by the grain angle and the creation of the closed loop of solutions from the branch of interface shapes with wavelengths 2λ. When a grain angle of only $6°$ was introduced the solution families were shifted substantially from the perfect results, but still exhibited the same sequence of shapes seen for $s=0$. Past the limiting value of G, the in-
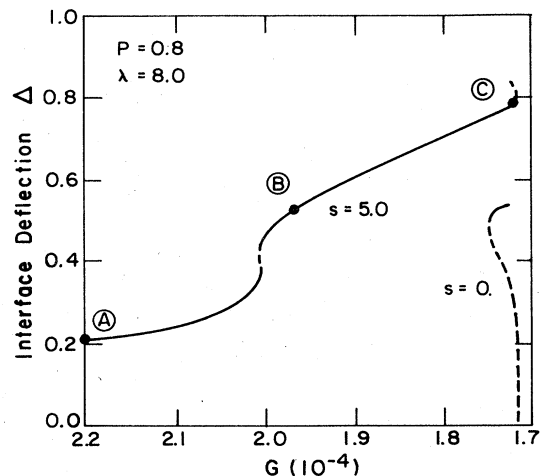

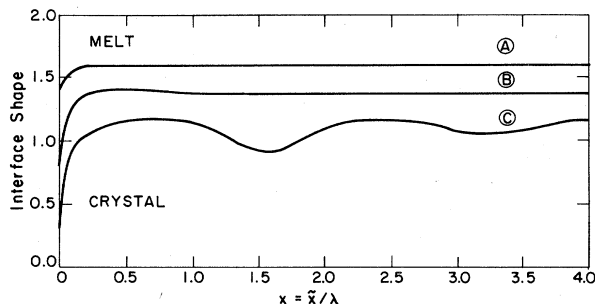FIG. 7. Interface family evolving from high values of G for $\lambda=8$ and $s=5.0$ $(89°)$.

FIG. 8. Sample interface shapes for $s = 5.0$ and $2\lambda = 8$.

terfaces in the primary shape family were unstable as the family evolved with increasing temperature gradient; shapes in this region had deep grooves adjacent to the grain, but were almost flat by a distance 2λ away. Past a second limit point the shapes existed at lower values of G and regained stability. Shapes on this branch were almost identical for $0 \leq x \leq \lambda$ to those calculated for grains spaced only λ apart, as shown by the representative interface shapes in Fig. 6.

The family of interface shapes computed with grains of angle with $s = 5.0$ and space $2\lambda = 8$ apart are represented in Fig. 7, and sample interface shapes are shown in Fig. 8. For $G = 1.718 \times 10^{-4}$, just above the critical value $G = G_c$, the interface undulated with a wavelength of about $\lambda / 2$. The peak next to the grain boundary was only slightly more pronounced than ones farther away. Calculations at lower temperature gradients were stopped by the limit point created by the rupturing of the secondary bifurcation to shapes with wavelength 2λ; see the results for $s = 0.1$ in Fig. 5. Attempts to compute around this limit failed for $s = 5.0$.

V. DISCUSSION

Grain boundaries along a melt/solid interface disrupt the symmetry of the cellular forms created by morphological instability and cause imperfections in the connectivity of the families of interfaces originating at bifurcation points. These imperfections have been demonstrated both in the asymptotic analysis, valid for small interface deflections and for small grain angles, and in finite-element calculations of moderate-amplitude cellular shapes. The interpretation of the role of grain boundaries in the onset of morphological instability depends on whether the branching from the planar interface ($s = 0$) is subcritical or supercritical with respect to the control parameter, taken here as the temperature gradient G.

For supercritical bifurcation, introducing grain boundaries reduces the structure to a continuous family that evolves initially toward lower values of G; the sharp transition to cellular interfaces for $s = 0$ is replaced by a smooth evolution of undulation along the interface. The bifurcation point for subcritical bifurcation is replaced by a limit point in G at which a discontinuous change in the

stable interface must occur. The value of temperature gradient for the location of this limit point is extremely sensitive, $O(s^{2/3})$ for $s \ll 1$. This last scaling explains the preferential development of undulations near grain boundaries observed in experiments.

Introducing grain boundaries also destroys secondary bifurcation points located for the perfect case ($s = 0$) and creates secondary limit points at moderate-amplitude interface shapes. The presence of these limits severely complicates the tracing of interface families; without the calculations of interfaces containing no grain boundaries, the interpretation of the results in Sec. IV would be almost impossible.

Grain boundaries are imperfections in any model for solidification which yield steady bifurcations from a planar interface. The $O(s^{2/3})$ dependence of the displacement of the limit point created from a subcritical bifurcation holds for the model used by Mullins and Sekerka that includes variations in the temperature field and for the analysis of Coriell et al.[19] that includes the onset of thermosolutal convection in the vicinity of the interface. Cellular forced convection against the interface can be an independent mechanism for rupturing the bifurcating families. Fluid motion adjacent to the interface will cause lateral solute segregation which deforms the interface and breaks the symmetry just as the grain angle does. The combination of grain boundaries and nonuniform convection which always exist in experimental systems make it extremely doubtful that the sudden changes in interface shape predicted by theories which neglect these imperfections can ever be strictly observed.

Although the finite-element calculations have demonstrated the onset of undulations in the interface near the grain angle, the large-amplitude undulations depicted in Ref. 10 were not found along the family of stable shapes. This difference may be explained either by differences in the physics of solidification for the pure succinonitrile used in Ref. 10 and the dilute binary system studied here, or in the narrow range of $|G - G_c|$ computed here. The undulations in interface shape shown in Fig. 8 do result in large variations in the solute concentration along the solidifying front which are easily computed from Eq. (2.5). For the most deformed interface shown in Fig. 8, the concentration calculated at the grain boundary was 30% above that far from the grain boundary, while the concentration at the first peak was 4% below the far field value. These undulations in composition are observed experimentally as solute bands by etching slices of the crystal, as demonstrated in Ref. 9.

ACKNOWLEDGMENTS

*To whom correspondence should be addressed.

[1] W. W. Mullins and R. F. Sekerka, J. Appl. Phys. **34**, 323 (1963).

[2] W. W. Mullins and R. F. Sekerka, J. Appl. Phys. **35**, 444 (1964).

[3] D. J. Wollkind and L. A. Segal, Philos. Trans. R. Soc. London, Ser. A **268**, 351 (1970).

[4] J. S. Langer, Rev. Mod. Phys. **52**, 1 (1980).

[5] G. B. McFadden and S. R. Coriell, Physica (Utrecht) (to be published).

[6] R. Sriranganathan, D. J. Wollkind, and D. B. Oulton, J. Cryst. Growth **62**, 265 (1983).

[7] G. I. Sivashinsky, Physica (Utrecht) **8D**, 243 (1983).

[8] L. H. Ungar and R. A. Brown, Phys. Rev. B **29**, 1367 (1984).

[9] L. R. Morris and W. C. Winegard, J. Cryst. Growth **5**, 361 (1969).

[10] R. J. Schaefer and M. E. Glicksman, Metall. Trans. **1**, 1973 (1970).

[11] T. Sato and G. Ohira, Trans. Jpn. Inst. Met. **12**, 285 (1971).

[12] J. D. Ayers and R. J. Schaefer, in *Solidification and Casting of Metals* (Metals Society, London, 1979).

[13] S. R. Coriell and R. F. Sekerka, J. Cryst. Growth **19**, 90 (1973).

[14] S. R. Coriell and R. F. Sekerka, J. Cryst. Growth **19**, 285 (1973).

[15] J. P. Keener and H. B. Keller, Arch. Ration. Mech. Anal. **50**, 159 (1973).

[16] B. J. Matkowsky and E. L. Reiss, SIAM (Soc. Ind. Appl. Math.) **33**, 230 (1977).

[17] L. H. Ungar and R. A. Brown, Philos. Trans. R. Soc. London, Ser. A **306**, 324 (1982).

[18] P. Hall and I. C. Walton, J. Fluid Mech. **90**, 377 (1979).

[19] S. R. Coriell, M. R. Cordes, W. J. Boettinger, and R. F. Sekerka, J. Cryst. Growth **49**, 13 (1980).